Lattice Mismatch Dislocations in a Preferentially Sputtered Alloy Studied by Scanning Tunneling Microscopy

M. Schmid, A. Biedermann, H. Stadler, and P. Varga
Institut für Allgemeine Physik, Technische Universität Wien, A-1040 Wien, Austria
(Received 9 March 1992)

Scanning tunneling microscopy (STM) on a sputtered and annealed $Pt_{25}Ni_{75}(111)$ single crystal reveals a network of subsurface lattice mismatch dislocations caused by platinum enrichment due to preferential sputtering and recoil mixing. Atomically resolved STM topographs are compared with simulations of these dislocations using embedded atom potentials. This allows one to estimate the depth of the dislocations, and thus the thickness of Pt enrichment, which is three monolayers on the 500 eV Xe^+ sputtered and five monolayers on the Ar^+ sputtered surface, compatible with the depth of radiation damage.

PACS numbers: 61.70.Jc, 61.80.Jh, 68.35.Dv, 68.35.Fx

Lattice mismatch is a frequent phenomenon in the growth of thin films, where dislocations caused by the different lattice constants of substrate and film have been observed by transmission electron microscopy [1,2] and scanning tunneling microscopy (STM) [3,4]. In the present Letter we show for the first time a case of lattice mismatch dislocations which is due to enrichment of one alloy component by sputtering, and we are able to employ atomically resolved STM topographs for a full characterization of this dislocation system. Determination of dislocation density and comparison with simulations of individual dislocations yield both the composition and the thickness of the enriched layer. This offers a totally new method of surface analysis for such systems, based entirely on geometrical information.

The STM analysis has been performed with a customized commercial instrument (Omicron micro-STM). Preparation and STM work were done in the same ultrahigh vacuum chamber with a base pressure below 1×10^{-10} mbar. For sputtering a 500 eV Ar or Xe beam inclined 70° to the surface normal was used, yielding a current density of 0.7 $\mu A/cm^2$. The sample was cleaned by repeated cycles of sputtering and annealing until no contaminations were detectable by low-energy ion-scattering spectrometry (LEIS) below 770 K, and approximately 1% of a monolayer of sulfur at 1000 K. After annealing above 970 K the crystal showed large terraces separated by nearly straight and parallel monatomic steps and no dislocations.

If the crystal is sputtered with a dose of some 10^{16} ions cm^{-2} and annealed thereafter at temperatures between 600 and 870 K, shallow ditches 0.2–0.5 Å deep and 20–50 Å wide appear on the surface. Some ditches run along or across monatomic steps without being influenced by the steps, which makes a pure surface phenomenon (restricted to the first layer) implausible. With higher ion dose, the number of these ditches grows, and they form a network of hexagons with triangles at their edges, as shown in Fig. 1. The contrast is mainly topographical, since $I(z)$ measurements and variation of the tunneling voltage between ±0.5 mV and 10 V did not show any evidence of electronic (density of state) effects. STM images after oxygen adsorption did not show any differences between ditches and the flat regions, which would indicate different chemical composition [6].

Atomic resolution topographs (Fig. 2) show that surface atomic order is preserved on the ditches. At the ends of the ditches dislocations reach the surface [Fig. 2(a)]. This means that the ditches are a result of subsurface dislocations. The sense of the Burgers vectors, determined from Burgers circuits [7] as shown in Fig. 2, always implies that there are fewer atoms in the upper monolayers than below the dislocation lines; thus the upper monolayers have a larger lattice constant than the bulk. Since the lattice constant of Pt_xNi_{1-x} alloys increases with the Pt concentration, this indicates platinum enrichment in the upper layers. We can exclude contaminations as a reason for the larger lattice constant of the upper monolayers (Auger electron spectrometry shows no contaminations).

We have thoroughly investigated the dislocation system by atomically resolved STM topographs. If we have a "perfect" subsurface dislocation network, as in the left

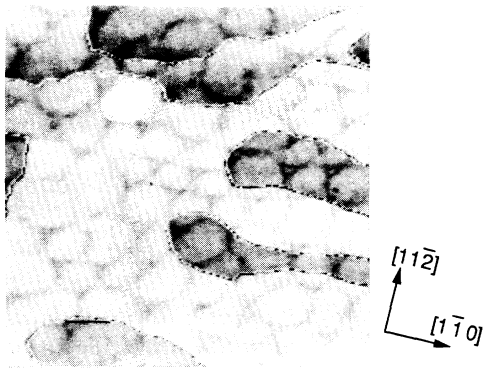

FIG. 1. STM topograph (1000 Å×1000 Å) of the $Pt_{25}Ni_{75}(111)$ surface after Xe sputtering with 6×10^{16} ions cm^{-2} and annealing to 750 K. In addition to monatomic steps, which are remnants of the sputter-induced roughness [5], shallow ditches appear on the surface. For improved contrast of the ditch pattern, the terrace height levels have been nearly equalized by image processing, leading to noise at the steps.

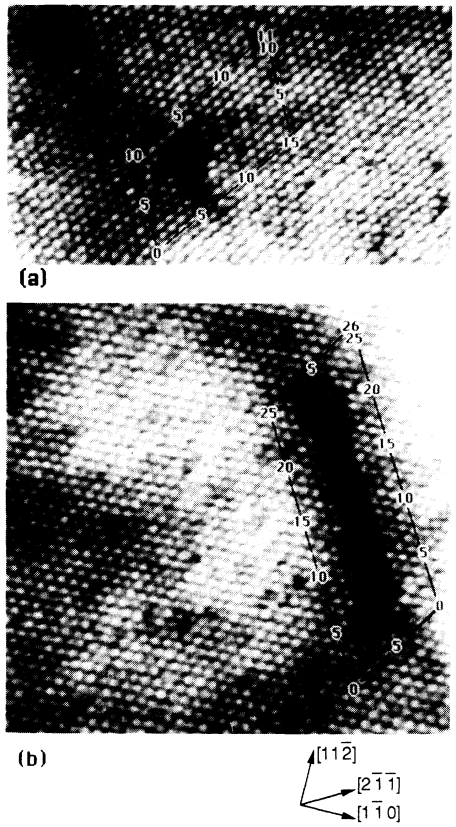

FIG. 2. Atomically resolved constant current topographs of the sputtered and annealed surface. (a) Lower (ditch) regions in the left part of the picture, ending in a dislocation (classified as type A in Fig. 3). (b) Two Shockley partial dislocations span a $\frac{1}{3}$ monatomic step (type C); subsurface dislocations extending from the ends of this step are visible as shallow ditches. [An averaged section profile through the $\frac{1}{3}$ step, where a $(1\bar{1}\bar{1})$ stacking fault plane intersects the surface, is shown in Fig. 5.] Burgers circuits around the dislocation cores are shown for easy determination of the total Burgers vector reaching the surface, which is $\frac{1}{2}$ $[0\bar{1}1]$ in both images. For both images the crystal has been sputtered with 500 eV Ar^+ and annealed at 750 K. Image size (horizontally) is 100 Å, tunneling conditions (voltage/current) are 0.5 mV/7.5 nA for the top frame and 4 mV/18 nA for the bottom frame. Slight high-pass filtering is used to enhance the contrast of the atomic corrugation.

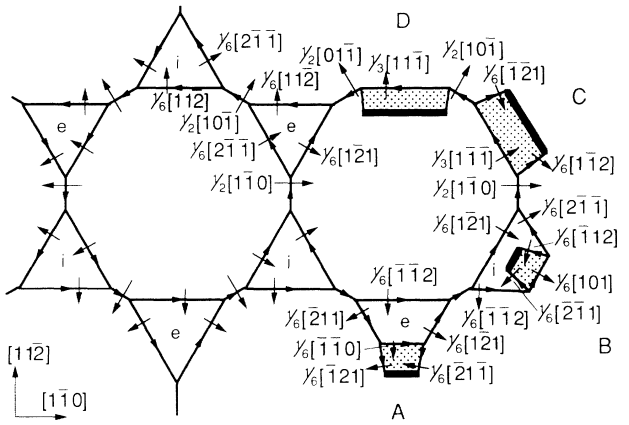

FIG. 3. Subsurface lattice mismatch dislocation network on the (111) plane. Burgers vectors are drawn as arrows crossing the respective dislocation line, the sense of which is indicated. Letters *i* and *e* indicate triangular regions containing intrinsic and extrinsic stacking faults parallel to the surface, while the shaded areas are intrinsic stacking fault planes oriented in the $(\bar{1}\bar{1}1)$, $(\bar{1}1\bar{1})$, $(1\bar{1}\bar{1})$, and $(\bar{1}\bar{1}1)$ directions in cases A, B, C, and D, respectively. Bold lines mark the intersection of these inclined stacking fault planes with the surface, where steps with a height $\frac{1}{3}$ of a monatomic step appear. For clarity, the size of the shaded areas has been exaggerated. The dislocation systems A and C (B and D) occupy equivalent sites. Dislocations of type $\frac{1}{2}$ ⟨110⟩ and $\frac{1}{3}$ ⟨111⟩ may split into partials.

part of Fig. 3, no dislocations reach the surface, and we only see ditches above the dislocations. Perfect dislocations of the $\frac{1}{2}$ ⟨110⟩ type split into Shockley partials forming extended nodes enclosing triangular regions. Analysis of the Burgers vectors associated shows that the triangles contain either intrinsic (stacking sequence *ABCBC*, marked "*i*" in Fig. 3) or extrinsic (*ABCBABC*, marked "*e*") stacking faults [7] dependent on their orientation. Imperfections of this pattern appear as dislocations reaching the surface; three different cases (A, B, and C) thereof have been observed by STM. In each case the total Burgers vector reaching the surface is of the $\frac{1}{2}$ ⟨110⟩ type, split into partials spanning an intrinsic stacking fault plane inclined 70.5° to the surface (shaded in Fig. 3).

In cases A [Fig. 2(a)] and B the stacking fault planes intersect in a stair-rod partial dislocation of $\frac{1}{6}$ ⟨110⟩ type forming an obtuse angle of 109.5° or an acute angle of 70.5°, respectively. The length of the inclined fault plane between the two partial dislocations reaching the surface is typically 10–15 Å in these cases. In case C, which occurs at a site equivalent to A, the ditch pattern of the STM topographs [e.g., Fig. 2(b)] suggests that the (extrinsic) stacking fault triangle totally disappears, which would lead to a $\frac{1}{3}[1\bar{1}\bar{1}]$ dislocation. Both the b^2 criterion [7] and our simulations described below indicate that this dislocation splits into the partials $\frac{1}{6}$ $[2\bar{1}\bar{1}]+\frac{1}{6}$ $[0\bar{1}\bar{1}]$, thereby forming an intrinsic stacking fault in a plane parallel to the surface, as shown in Fig. 4. This stacking fault is outside of the hexagon (below the shaded plane in Fig. 3), therefore its size is limited not only by its own areal energy, but also by the tension of the adjacent $\frac{1}{2}$ $[10\bar{1}]$ and $\frac{1}{2}$ $[1\bar{1}0]$ dislocations. The length of the inclined fault plane at the surface is typically 50 Å in case C.

We have never observed case D, which would be similar to C, but with an intrinsic stacking fault triangle disappearing. The $\frac{1}{3}$ $[11\bar{1}]$ dislocation would split into partials again, forming just this intrinsic stacking fault situated inside the hexagon (below the shaded plane in Fig. 3). In this case, however, the tension of the adjacent ⟨110⟩-type dislocations would further separate the partials of the $\frac{1}{3}$ $[11\bar{1}]$ dislocation, increasing the intrinsic

stacking fault area and thereby forming type B. Thus at sites equivalent to B or D, only the dislocation system B will appear.

For the simulations a molecular dynamics code using embedded atom potentials [8] has been employed. Various slabs have been examined, each of them with a total thickness of thirty layers, n_1 surface layers containing 50% Pt, n_2 layers below with 37.5% Pt, and all other layers were assumed to have bulk composition, i.e., 25% Pt. Since LEED did not show any indications of chemical order at the surface, the two species were distributed randomly within these layers, although $Pt_{25}Ni_{75}$ and $Pt_{50}Ni_{50}$ are known to form ordered phases [9]. Dislocations were forced into these crystals by removing rows of atoms from the upper n layers, and the resulting configuration was relaxed at $T=0$ K using the molecular dynamics code.

Simulations of $\frac{1}{2}\langle 110\rangle$-type dislocations, which are mainly responsible for the ditches at low ion dose, have shown that the width and depth of the ditches are in the same range as determined by STM, but they strongly depend on the separation distance of the Shockley partials, into which $\frac{1}{2}\langle 110\rangle$ dislocations split. This distance depends critically on the parameters used for the simulations (temperature, potentials). STM data also show that sections through these ditches vary in width and corrugation, even within a single image. We therefore do not employ these data for further analysis.

Results of simulating a section through the dislocation system C (Figs. 2 and 3) are shown in Figs. 4 and 5. To reduce "noise" coming from the statistical arrangement of Pt and Ni atoms, the positions of five atoms behind each other (i.e., along $[01\bar{1}]$) have been averaged to create the section in Fig. 4 and the first-layer positions in Fig. 5. Again, the separation of the partials ($\frac{1}{6}$ $[2\bar{1}\bar{1}]$ and $\frac{1}{6}$ $[0\bar{1}\bar{1}]$), which can be controlled by means of the concentration profile, determines whether a depression (ditch) is formed on the surface surrounding the dislocation system. The immediate vicinity of the inclined stacking fault depends mainly on the depth n of the dislocation core; i.e., for small n, lattice relaxation tends to reduce the height of the $\frac{1}{3}$ step and further makes the surface profile more symmetrical. This behavior is insensitive to the separation of the partials mentioned above, since it is mainly determined by the size of the inclined stacking fault plane. Further simulations indicate that the section profiles are insensitive to the Pt concentration in the upper layers, as long as the shape of the concentration profile remains similar.

Figure 5 also shows two STM line scans through type-C dislocation systems, which have been averaged along $[0\bar{1}\bar{1}]$ to reduce fluctuations caused by the random arrangement of the two different species. A rough comparison with the different calculated data shows that the Xe sputtered sample has a more symmetric appearance (n between 2 and 4), while the Ar sputtered case is expected to fit $n=4$ or slightly higher. For the Ar sputtered surface we have found the best agreement with the simulation for $n=5$ ($n_1=3$, $n_2=2$).

Having determined the Burgers vectors (Fig. 3), we may calculate the amount of lattice mismatch from the density of subsurface dislocation lines (ditches), which increases with the ion dose until it remains constant at ion doses greater than 10^{17} cm^{-2} ("steady-state" conditions). Since the dependence of dislocation density on ion dose shows hardly any threshold at low dose, lateral stress in the surface layers must be rather low. Therefore assuming unstrained surface layers, we can use Vegard's rule to calculate the platinum concentration in these layers as (43 ± 2)% in steady state (the error estimate reflects uncertainties counting dislocations in wide area scans). This value agrees excellently with (47 ± 5)% Pt determined by Auger electron spectrometry (AES) and

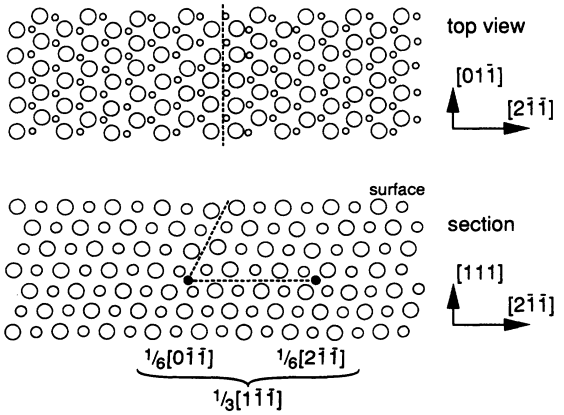

FIG. 4. Atom positions calculated for the dislocation system C, assuming dislocation cores at a depth of $n=4$ layers. Broken lines mark stacking fault planes and the two black dots indicate dislocation cores, whose Burgers vectors are given below each of them.

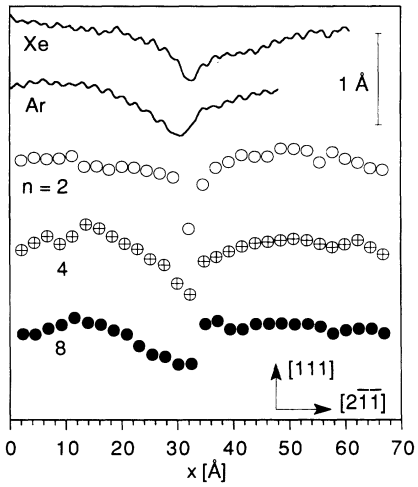

FIG. 5. First-layer atom positions calculated for the dislocation system C, using different depths n of the dislocation core (concentration profile $n_1=n_2=n/2$). The two lines are STM scans through such dislocations on the surface sputtered with high doses of 500 eV Xe and Ar, respectively.

$(41 \pm 3)\%$ measured by LEIS on the sputtered (not annealed) surface.

The dependence of dislocation density (and thus composition) on the ion dose clearly identifies preferential sputtering as the reason for the Pt enrichment. After annealing to temperatures below 870 K, the density of dislocations (ditches) remains constant, indicating constant composition. This has apparently been misinterpreted previously as thermodynamic equilibrium [10], leading to misinterpretations of the Pt enrichment as multilayer segregation [11]. After annealing to higher temperatures, the dislocation density decreases, and falls to zero above 970 K, where diffusion coefficients [12] suggest rapid equilibration. All measurements of surface composition after annealing at these temperatures indicate monolayer segregation [13] or alternating monolayers of Pt and Ni enrichment [14], both of which cannot form the dislocation system described in this Letter.

We have performed simulations of the sputtering process using the TRIDYN code [15] to find the depth of radiation damage caused by the Ar and Xe ions. In the case of Ar sputtering, 95% of all damaging energy is deposited within the first six monolayers, and in the case of Xe within the first three layers. This agrees well with the thickness of the Pt-enriched layer determined above. Thus we conclude that the multilayer Pt enrichment is formed during sputtering by recoil mixing and not by radiation-damage-enhanced diffusion during annealing (which would need a thicker damaged layer as a source for the Pt transported to the surface).

We conclude that we have found good agreement between experimental results from STM and conventional surface analysis, simulations of the dislocations, and a variety of other data. Therefore the study of lattice mismatch dislocations, wherever they occur, should be regarded as a new and powerful tool for the investigation of multilayer compositional changes in surface physics. In this special case of PtNi, which has been intensively studied previously [16] due to its importance for heterogeneous catalysis, we could solve the open question of monolayer versus multilayer segregation and we could demonstrate the effectiveness of recoil mixing by sputtering even at the low ion energy of 500 eV and very flat incidence. The existence of mismatch dislocations in sputtered alloy surfaces, which has been revealed by this work, may have important consequences to the processes of sputtering and subsequent annealing, such as providing diffusion pipes for implanted atoms.

The authors are very grateful to Stephen Foiles (Sandia National Laboratories, Livermore) for supplying us with the computer code and for his substantial help in implementing the embedded atom method and to G. S. Sohal, who provided the crystal. We would further like to thank G. Betz, W. Hofer, P. Novacek, and P. Weigand for many helpful discussions. This work was supported by the "Fonds zur Förderung der Wissenschaftlichen Forschung" (Austrian Science Foundation) under projects No. P6912 and No. P8147.

[1] K. Yaki, K. Tobayashi, Y. Tanishiro, and K. Takayanagi, Thin Solid Films **126**, 95 (1985).
[2] R. T. Tung and F. Schrey, Phys. Rev. Lett. **63**, 1277 (1989).
[3] R. Stalder, H. Sirringhaus, N. Onda, and H. Känel, Appl. Phys. Lett. **59**, 1960 (1991); Surf. Sci. **258**, 153 (1991).
[4] G. O. Pötschke and R. J. Behm, Phys. Rev. B **44**, 1442 (1991).
[5] T. Michely, K. H. Besocke, and G. Comsa, Surf. Sci. **230**, L135 (1990).
[6] P. Novacek and P. Varga, Surf. Sci. **248**, 183 (1991).
[7] J. P. Hirth and J. Lothe, *Theory of Dislocations* (Wiley, New York, 1982), 2nd ed.
[8] S. M. Foiles, M. I. Baskes, and M. S. Daw, Phys. Rev. B **33**, 7938 (1986); **37**, 10378(E) (1988).
[9] C. E. Dahmani, M. C. Cadeville, J. M. Sanchez, and J. L. Morán-López, Phys. Rev. Lett. **55**, 1208 (1985).
[10] L. De Temmermann *et al.*, Surf. Sci. **178**, 888 (1986).
[11] L. De Temmermann, C. Creemers, H. Van Hove, and A. Neyens, Surf. Sci. **183**, 565 (1987).
[12] *Metal Reference Book,* edited by C. J. Smithells (Butterworths, London, 1976), 5th ed.
[13] J. C. Bertolini *et al.*, Surf. Sci. **119**, 95 (1982).
[14] Y. Gauthier *et al.*, Surf. Sci. **162**, 342 (1985); Y. Gauthier, Y. Joly, R. Baudoing, and J. Rundgren, Phys. Rev. B **31**, 6216 (1985); R. Baudoing, Y. Gauthier, M. Lundberg, and J. Rundgren, J. Phys. C **19**, 2825 (1986).
[15] W. Möller and W. Eckstein, Nucl. Instrum. Methods Phys. Res., Sect. B **2**, 814 (1984).
[16] *Surface Segregation Phenomena,* edited by P. A. Dowben and A. Miller (CRC, Boca Raton, 1990), and references therein.

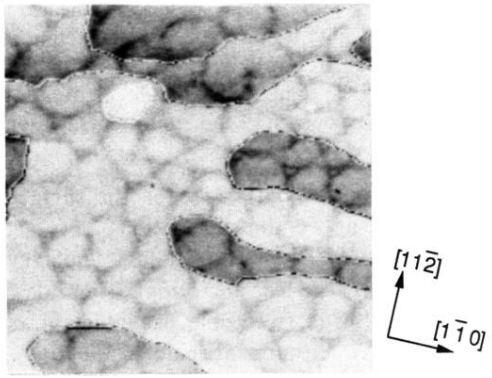

FIG. 1. STM topograph (1000 Å×1000 Å) of the $Pt_{25}Ni_{75}(111)$ surface after Xe sputtering with 6×10^{16} ions cm^{-2} and annealing to 750 K. In addition to monatomic steps, which are remnants of the sputter-induced roughness [5], shallow ditches appear on the surface. For improved contrast of the ditch pattern, the terrace height levels have been nearly equalized by image processing, leading to noise at the steps.

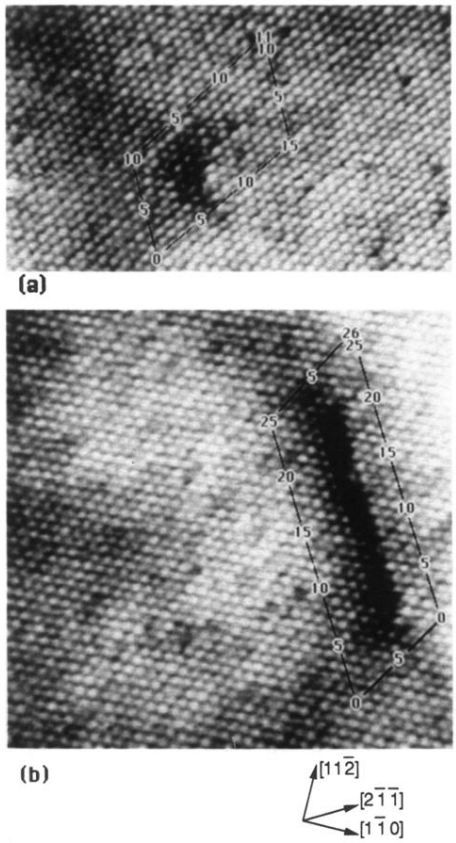

FIG. 2. Atomically resolved constant current topographs of the sputtered and annealed surface. (a) Lower (ditch) regions in the left part of the picture, ending in a dislocation (classified as type A in Fig. 3). (b) Two Shockley partial dislocations span a $\frac{1}{3}$ monatomic step (type C); subsurface dislocations extending from the ends of this step are visible as shallow ditches. [An averaged section profile through the $\frac{1}{3}$ step, where a $(1\bar{1}\bar{1})$ stacking fault plane intersects the surface, is shown in Fig. 5.] Burgers circuits around the dislocation cores are shown for easy determination of the total Burgers vector reaching the surface, which is $\frac{1}{2}$ $[0\bar{1}1]$ in both images. For both images the crystal has been sputtered with 500 eV Ar^+ and annealed at 750 K. Image size (horizontally) is 100 Å, tunneling conditions (voltage/current) are 0.5 mV/7.5 nA for the top frame and 4 mV/18 nA for the bottom frame. Slight high-pass filtering is used to enhance the contrast of the atomic corrugation.